Applied Geochemistry 63 (2015) 222–234

Contents lists available at ScienceDirect

Applied Geochemistry

journal homepage: www.elsevier.com/locate/apgeochem

Persistent U(IV) and U(VI) following in-situ recovery (ISR) mining of a sandstone uranium deposit, Wyoming, USA

T.J. Gallegos [a, *], K.M. Campbell [b], R.A. Zielinski [c], P.W. Reimus [d], J.T. Clay [e], N. Janot [f, 1], John R. Bargar [g], William M. Benzel [h]

[a] U.S. Geological Survey, 12201 Sunrise Valley Drive, Mail Stop 956, Reston, VA, 20192, USA
[b] U.S. Geological Survey, 3215 Marine Street, Suite E-127, Mail Stop 496, Boulder, CO, 80303, USA
[c] U.S. Geological Survey, Box 25046, Denver Federal Center, Mail Stop 939, Denver, CO, 80225, USA
[d] Los Alamos National Laboratory, P.O. Box 1663, Mail Stop J966, Los Alamos, NM, 87545, USA
[e] Cameco Resources, 550 N. Poplar St., Ste 100, Casper, WY, 82601, USA
[f] Stanford Synchrotron Radiation Lightsource, Bldg 137, 2575 Sand Hill Rd., Menlo Park, CA, 94025, USA
[g] Stanford Synchrotron Radiation Lightsource, Bldg 137, MS 69, 2575 Sand Hill Rd., Menlo Park, CA, 94025, USA
[h] U.S. Geological Survey, Box 25046, Denver Federal Center, Mail Stop 973, Denver, CO, 80225, USA

ARTICLE INFO

Article history:
Received 6 May 2015
Received in revised form
27 August 2015
Accepted 29 August 2015
Available online 31 August 2015

Keywords:
Uranium
In-situ recovery
ISR
Uranium mining
Sandstone-hosted uranium deposit
Groundwater restoration

ABSTRACT

Drill-core samples from a sandstone-hosted uranium (U) deposit in Wyoming were characterized to determine the abundance and distribution of uranium following in-situ recovery (ISR) mining with oxygen- and carbon dioxide-enriched water. Concentrations of uranium, collected from ten depth intervals, ranged from 5 to 1920 ppm. A composite sample contained 750 ppm uranium with an average oxidation state of 54% U(VI) and 46% U(IV). Scanning electron microscopy (SEM) indicated rare high uranium (~1000 ppm U) in spatial association with P/Ca and Si/O attributed to relict uranium minerals, possibly coffinite, uraninite, and autunite, trapped within low permeability layers bypassed during ISR mining. Fission track analysis revealed lower but still elevated concentrations of U in the clay/silica matrix and organic matter (several 10 s ppm) and yet higher concentrations associated with Fe-rich/S-poor sites, likely iron oxides, on altered chlorite or euhedral pyrite surfaces (but not on framboidal pyrite). Organic C (<1.62%), total S (<0.31%), and P (<0.03%) were in low abundance relative to the overall bulk composition. Microbial community analysis showed a diverse group of bacteria present with a wide range of putative metabolisms, and provides evidence for a variety of redox microenvironments co-existing in core samples. Although the uranium minerals persisting in low permeability areas in association with organic carbon were less affected by oxidizing solutions during mining, the likely sequestration of uranium within labile iron oxides following mining and sensitivity to changes in redox conditions requires careful attention during groundwater restoration.

Published by Elsevier Ltd.

1. Introduction

In situ recovery (ISR) is currently the primary method of uranium extraction in the United States and accounts for 45% of global uranium (U) production (World Nuclear Association, 2014). Uranium ISR is a solution mining technique that involves the injection of a leaching solution, or 'lixiviant', into a permeable sandstone-hosted uranium deposit in an aquifer confined between two low-permeability aquitards. The lixiviant often consists of native groundwater mixed with an oxidant (e.g., $O_2(g)$) and a complexing agent ($CO_2(g)$). The O_2 oxidizes U(IV) minerals to U(VI) and the dissolved carbonate complexes the U(VI) to form uranyl dicarbonate, $UO_2(CO_3)_2^{2-}$, and other uranyl carbonate complexes, including ternary uranyl-calcium-carbonate complexes (Langmuir, 1979), dissolving the uranium. The resulting uranium-rich groundwater solution is then pumped to the surface where the

* Corresponding author.
E-mail addresses: tgallegos@usgs.gov (T.J. Gallegos), kcampbell@usgs.gov (K.M. Campbell), rzielinski@usgs.gov (R.A. Zielinski), preimus@lanl.gov (P.W. Reimus), James_Clay@cameco.com (J.T. Clay), noemie.janot@univ-lorraine.fr (N. Janot), bargar@slac.stanford.edu (J.R. Bargar), wbenzel@usgs.gov (W.M. Benzel).
[1] Current contact information: Laboratoire Interdisciplinaire des Environnements Continentaux (LIEC), UMR 7360 CNRS-Université de Lorraine, 15 Avenue du Charmois, F-54500, Vandoeuvre, France. noemie.janot@univ-lorraine.fr

http://dx.doi.org/10.1016/j.apgeochem.2015.08.017
0883-2927/Published by Elsevier Ltd.

uranium is removed by ion exchange, concentrated and treated with a strong acid (typically HCl or H_2SO_4) and precipitated in a series of minerals called "yellowcake" (including $UO_4 \cdot 2H_2O$, U_3O_8, and various U(VI) oxides), the product of uranium mining. Following ISR, groundwater restoration of the host aquifer is required to lower the elevated concentrations of uranium and other trace elements associated with the uranium deposit such as As, Se, and Ra back to pre-mining groundwater quality. Often groundwater remediation occurs in several steps. First, one or more pore volumes of water from the mining zone are pumped and either disposed of or treated and replaced by groundwater drawn in from outside of the mining zone (termed "groundwater sweep"). Subsequently, several pore volumes of water (sometimes greater than 15 pore volumes) are extracted, treated by reverse osmosis, and recirculated (Davis and Curtis, 2007). Reverse osmosis treatment is sometimes followed by the addition of a chemical reductant (such as sodium sulfide) or less commonly by bio-stimulation whereby a nutrient such as sodium acetate is added to encourage the proliferation of metal-reducing bacteria. This last step is done with the intention of reversing the oxidation of aquifer solids that are the result of mining as well as removing residual dissolved heavy metals. The regulatory target for restoration is the attainment of pre-mining baseline values for the concentrations of a suite of species that include the previously cited trace elements and a variety of other elements, ions, and total dissolved solids (TDS). Active restoration operations are generally followed by a stabilization period in which the groundwater quality is monitored to assure that the groundwater has been remediated to an acceptable standard (Davis and Curtis, 2007).

Although groundwater sweeping followed by reverse osmosis (RO) treatment is thought to be a highly efficient method of remediation (Borch et al., 2012), achieving pre-mining water quality goals for some elements is difficult (Catchpole and Kuchelka, 1993; Darling, 2008; Davis and Curtis, 2007; Hall, 2009; Vogt et al., 1984). In some cases, the concentrations of uranium and other constituents, namely Se, As, Ra, Mn, Fe and sulfate are initially lowered by the remediation process, but rebound to higher values during or after recirculation (Davis and Curtis, 2007), in part, due to mixing and back-diffusion of unrestored water from low permeability zones (Power Resources Inc, 2004). Geochemical modeling has also suggested that at least a portion of the rebound may be due to increased oxidation of aquifer solids, which poises system redox to higher than pre-mining levels and keeps elements of concern dissolved, based on estimates of post-mining mineralogy (Davis and Curtis, 2007). Although it is generally accepted that during ISR, the uranium, along with reductants such as pyrite and marcasite become oxidized, the extent of oxidation is unknown (Davis and Curtis, 2007). This is important because the persistence of residual reductants, including iron sulfides, organic carbon, and/or dissolved ferrous iron and sulfide could facilitate groundwater restoration by re-establishing the reducing conditions necessary to reductively precipitate uranium and remove it from solution (Deutsch et al., 1985; Gallegos et al., 2013; Hyun et al., 2012; IAEA, 2005; Moyes et al., 2002, 2000; Wersin et al., 1994). For example, residual uranium found in a previously-mined and restored sandstone-hosted uranium deposit in the Powder River Basin at the Smith Ranch-Highland ISR mining site in Wyoming was correlated with carbonaceous material and clay in low-permeability strata and suggested that pyrite present in more permeable sections might provide for uranium attenuation through reductive deposition of uranium on partially altered pyrite (WoldeGabriel et al., 2014). Long-term natural attenuation of reduced uranium minerals such as $UO_2(s)$ could prevent dissolved uranium from being transported outside of the mined area (Borch et al., 2012). However, there is a need to better understand extent of oxidation and primary or secondary mineral phases that may be controlling the residual concentrations of uranium in groundwater following ISR.

The objective of this work is to characterize the sediments in 0.3-m sections of drill core from a sandstone-hosted uranium deposit following ISR and groundwater restoration to: (1) determine the oxidation state and mode-of-occurrence of persistent uranium; (2) assess the leachability of persistent uranium by solutions that simulate a range of post-mining pore fluid compositions; and (3) identify solid phases and microbial populations in the leached ores that could potentially re-establish reducing conditions and possibly immobilize persistent dissolved uranium in the mining zone.

2. Materials and methods

2.1. Field site

The Smith Ranch-Highland (SRH) uranium mine is located in the southern Powder River Basin, Converse County, Wyoming (Dahl and Hagmaier, 2005) (Fig. A1(A)). Following in-situ recovery (ISR) mining and groundwater restoration, an 8.5 m core (7.62 cm diameter) was obtained from the uranium deposit located at a depth of 231.34–239.88 m below ground surface (see profile in Fig. A1(B)). The ore body is of the roll-front type and resides in a permeable, arkosic sandstone thought to be in the Fort Union Formation (Paleocene). U–Pb isotopic dating of ore samples taken elsewhere on the mine site indicates that mineralization occurred 2–2.5 million years ago (Santos and Ludwig, 1983). See Fig. A1(C) for a geologic map, modified from Love and Christiansen, 1985.

ISR operations were conducted from June, 2000 to September, 2005, by injecting groundwater enriched with $O_{2(g)}$ and $CO_{2(g)}$ into the uranium deposit, decreasing pH from ~7.6 to 6.47 (Table B1). Although Eh values were more difficult to measure, initial estimated pre-mining baseline oxidation-reduction potential (ORP) values between −300 and −150 mV increased to around +90 mV (relative to the platinum electrode used in a YSI model 556 handheld meter) after mining. The injected solution is designed to oxidize the uranium (IV) minerals, which consist mainly of coffinite ($U(SiO_4)_{1-x}(OH)_{4x}$) and uraninite (UO_2) (Stewart et al., 2000), to aqueous U(VI) and form uranyl carbonate complexes. These reactions increased bicarbonate concentrations by a factor of 3–4 (from the mid-to upper-100s to 600–700 mg HCO_3^-/L), and dissolved uranium concentrations from 0.02 to 0.1 mg/L before mining to as much as 50–300 mg/L during mining (Davis and Curtis, 2007). In the immediate vicinity of where the core was taken for this study, post-mining concentrations prior to restoration were 13.9 mg U/L (Table B1) and alkalinity was 314 mg/L as $CaCO_3$ at pH 6.47. Total inorganic carbon (TIC) was elevated following ISR largely because carbon dioxide was added as part of the ISR leaching solution. Likewise, elevated concentrations of chloride (113 mg/L) were due to the recirculation of water from the ion exchange process through the mining zone.

Groundwater restoration in Mine Unit 4 commenced in 2010, about five years after mining ended. Restoration is typically conducted on blocks of wells consisting of 15–20 production wells and about twice as many injection wells, which are all served by a common 'header house'. Initial groundwater treatment included a groundwater sweep, whereby approximately one pore volume of groundwater was pumped from the formation, treated via ion exchange to remove uranium and either recycled to the other restoration areas or sent to a deep well, permitted by the Environmental Protection Agency (EPA) through its Underground Injection Control (UIC) program, for disposal. Subsequently, groundwater was pumped to the surface and treated by reverse osmosis (RO) with recirculation of the RO permeate into the header-house injection wells until the electrical conductivity of the water returned to pre-mining

values. It is estimated that on average between 8 and 9 pore volumes were pumped and recirculated during groundwater restoration for each block of wells served by header houses within Mine Unit 4, following the initial groundwater sweep. Following groundwater restoration, mine records reported that uranium concentrations were lowered to between 0.42 and 0.6 mg/L U and alkalinity was lowered to 168–187 mg/L as $CaCO_3$ at pH 6.11.

2.2. Sample collection and preservation, preparation, and screening

Following groundwater restoration, in May 2012, ten 0.3-m sections of drill core were extracted from the mined/restored ore zone. Cores were preserved in the field by vacuum sealing and storing on ice before shipment to the lab within five days, where they were placed into an anaerobic chamber (95% N_2 and 5% H_2) for approximately one month prior to characterization. During field sampling, a ~50-g split from freshly extruded core was also subsampled for DNA analysis at each 0.6-m interval, placed in a sterile 50 mL polyethylene centrifuge tube, frozen in the field using liquid nitrogen, and stored on dry ice until placed in a −60 °C freezer in the laboratory. Gamma radiation (μR/h) readings were measured in the laboratory on the surface of each drill core sample using a Ludlum Model 19 MicroR ratemeter with an internally mounted scintillation detector (calibrated at the USGS reactor facility at the Denver Federal Center in 2009). In most natural ore deposits, total gamma radiation is predominantly attributed to emissions from uranium and its decay products.

Individual drill core sections were prepared for characterization by disaggregating with a mortar and pestle and thoroughly mixing the predominantly sand-sized material to obtain a representative homogenized sample inside of a 5%H_2/95%N_2 anaerobic chamber (PlasLabs). A weight-averaged composite sample consisting of only the permeable strata likely to contact lixiviant solutions was also made by combining and homogenizing a 30-g split of each of the representative samples from each of the permeable core sections (all core sections except samples 7 and 8A, which were composed of a substantially harder material that could not be homogenized while maintaining anaerobic preservation, and were considered relatively impermeable). Polished thin sections were prepared on select intact cores using a clear epoxy impregnation for fission track radiography and microscopy analyses.

2.3. Solid phase characterization

Samples were characterized using scanning electron microscopy with energy dispersive X-ray spectroscopy (SEM-EDX, JEOL 5800LV), semi-quantitative X-ray diffraction (XRD, Scintag), electron microprobe (EMP, JEOL 8900 Electron Microprobe), and optical microscopy. The electron microprobe with a detection limit estimated at 300 ppm U was used to generate element distribution maps for concentrations of U, Fe, and S. Whole rock total carbon and total sulfur were measured by means of total combustion using infrared detection (Elementar) while total inorganic carbon was measured using titration coulometry. The difference between total carbon and inorganic carbon was assumed to be organic carbon. Whole rock major and trace elemental composition was measured by inductively coupled plasma-mass spectrometry, (ICP-MS, Perkin Elmer Elan 6100) and optical emission spectroscopy (ICP-OES, Perkin Elmer Optima 5300DV), after digestion of the sample with a $HF/HCl/HNO_3$ mixture. For fission track radiography, thin sections were bombarded with neutrons (U.S. Geological Survey TRIGA Nuclear Reactor) to induce fission of uranium, and the tracks of fission products were recorded on a detector material of muscovite mica. The fission track distribution in the mica was then photographed to produce the images. The radiographs were used to determine the distribution of trace amounts of uranium, which are below the detection limit of SEM-EDX or EMP (in this case, ~5 ppm–1000 ppm) (Zielinski and Budahn, 1998). Additionally, Sample 8B and Sample 4 containing 132 and 1920 ppm U, respectively, were analyzed by X-ray absorption near-edge spectroscopy (XANES, Stanford Synchrotron Radiation Lightsource (SSRL) in Menlo Park, CA) to determine the solid phase oxidation state of uranium. Uranium LII-edge fluorescence XANES spectra were measured at beamline 11-2 at SSRL, using a Si (220) double-crystal monochromator detuned to reject higher harmonic intensity. The samples were loaded in an Al sample holder with Kapton windows inside an anaerobic chamber (2–5% hydrogen, balance nitrogen). Immediately prior to analysis, the sample was mounted in a liquid N_2 cryostat, placed under vacuum and cooled to 77 K. Energy calibration was monitored continuously using a Mo foil and no drift in calibration was detected. XANES spectra were background subtracted, analyzed and fitted using ATHENA software (Ravel and Newville, 2005). Spectra of the samples were fitted using a linear combination of XANES spectra of uraninite (UO_2) and U(VI) adsorbed on ferrihydrite.

Samples were prepared for XRD by crushing samples to pass through a 250-μm sieve followed by a standard addition of 20% corundum ground with 4 mL of ethanol in a McCrone micronizing mill for 5 min (Eberl, 2003). After drying, the mixture was transferred to a plastic scintillation vial with 3 plastic balls along with a few drops of Vertrel® (Dupont) and shaken for 10 min. The powder was then passed through the sieve and subsequently side-loaded into an XRD sample holder. Samples were analyzed on a Scintag X-ray Diffractometer from 5 to 65° two-theta using Cu K-alpha radiation, with a step size of 0.02° two-theta, and a count time of two seconds per step using a scintillation counter.

Clay mineral identification was confirmed on the <8 μm fraction of the samples that were air-dried, ethylene glycolated, twice heat treated (400 and 550 °C for 1 h each), and mounted on oriented slides. XRD scans were collected ranging from 2 to 40° two-theta using Cu K-alpha radiation, with a step size of 0.03° two theta, and a count time of one second per step using a scintillation counter. Quantitative mineralogy was calculated using RockJock (Eberl, 2003), a computer program that determines quantitative mineralogy in powdered samples by comparing the integrated XRD intensities of individual minerals in complex mixtures to the intensities of an internal standard.

2.4. Microbial community analysis

Approximately 5 g of each frozen DNA sample was homogenized and DNA was extracted using a PowerSoil extraction kit (MoBio Laboratories). The 16S rRNA gene was amplified using 28F-519R bacterial primers and sequenced at the Research and Testing Laboratory (Lubbock, TX) on a Roche 454 FLX/FLX + platform with approximately 10,000 high-quality sequences returned per sample, providing excellent coverage of community diversity (Fig. A2). Sequence data was denoised, aligned, and analyzed with QIIME (Caporaso et al., 2010) using the SILVA database (Quast et al., 2013). Operational taxonomic units (OTUs) were defined as unique (97% sequence identity) and taxonomy grouped the genus level. Alpha diversity (diversity within each sample) was calculated using the Simpson metric, which determines the probability of the same taxa being selected twice during a random sampling of the data. A result close to 0 indicates a high diversity sample and a result close to 1 indicates low diversity. Beta diversity (diversity between samples) was calculated using a weighted UniFrac metric (Caporaso et al., 2010), which includes genetic distance and differences in taxonomic composition.

2.5. Batch leaching experiments

Samples with the highest uranium concentrations (4, 8B) and the composite were leached in order to determine operationally-defined solubility characteristics of residual uranium. Leaching solutions included: (1) 2.1 g/L H_2O_2 in deionized water (oxic with oxidant); (2) deionized water equilibrated in air (oxic DI); (3) deionized water equilibrated with an anoxic (95% N_2 and 5% H_2) atmosphere (anoxic DI); and (4) artificial groundwater equilibrated with the anoxic atmosphere (anoxic AGW). Artificial groundwater was made by approximating the major ion composition of an average pre-mining groundwater chemistry measured at the site (composition in Table B2). Anoxic leaching experiments were performed in an anaerobic chamber and oxic leaching experiments were conducted open to the atmosphere. A solid suspension of 200 g/L was produced by combining 20 g of disaggregated, homogenized sample with 100 mL of leachate. Leaching solutions were freshly prepared within 2 h prior to leaching, and anoxic solutions were prepared and equilibrated in the anaerobic chamber prior to sample addition. The pH, Eh, and specific conductance of the leach solutions were recorded before and after each experiment. Samples were mixed on a mechanical shaker for 24 h in HDPE Nalgene bottles. At the end of the 24-h leaching time, the leachates were filtered through a 0.7-μm glass fiber syringe filter in series with a 0.45 μm surfactant-free cellulose acetate syringe filter using a 60-mL plastic sterile luer-lok syringe. The recovered leachates were preserved for subsequent analysis of total trace elements by ICP-MS by acidifying to pH < 2 using ultra-pure nitric acid.

3. Results

3.1. Mineralogy

X-ray diffraction (XRD) analysis measures the crystalline portion of a sample. This does not include amorphous phases that may be present or organic components. XRD data were normalized to account for the crystalline phases only (Table B3). The detection limit for uranium minerals varies based on crystallinity factors and whether the strongest reflections from the phase have overlaps with other minerals in the assemblage. Typical detection limits for common uranium minerals are two or three weight percent, but may be as low as 0.5 or as high as five weight percent. For this sample set, all uranium minerals were below detection by XRD. The bulk mineralogy of the core samples was dominated by quartz (44–84%), K-feldspar (8–22%), and clays (up to ~40%), with smaller amounts of albite, generally consistent with the sandy texture of the more permeable layers sampled. The clay abundance was highly variable, with highest concentrations found in Samples 3, 7, and 8A. Clay minerals measured semi-quantitatively by XRD were dominated by smectite and mica (illite and muscovite), with smaller amounts of kaolinite and chlorite. Pyrite was also present in some samples, particularly in Samples 3 and 4, at concentrations between 0.1% and 0.3%. For the focus samples (4 and 8B), Sample 8B has more clay than Sample 4, while Sample 4 has more pyrite than Sample 8B. Total sulfur in all samples was relatively low (0.08–0.31%, Table B4), and carbon was primarily present as organic carbon (0.1–1.62%), with the highest inorganic carbon concentration in Sample 5 (0.11%) and most inorganic carbon concentrations at or below detection (0.01%) in all other samples. Phosphorous was present at <300 ppm (Table B4). Sample 4 contained 3.5 times more organic carbon and 2 times more sulfur than Sample 8B. Heterogeneity of the core samples was evident by the highly variable concentrations of total C, S, U, P, other trace elements (e.g., As, V; Table 1 and Table B4), and mineralogy, particularly the clay and pyrite content.

3.2. Uranium solid phase concentrations

Uranium persists in solid phases after the combined imposition of ISR mining and post-ISR groundwater restoration. Fig. A3 shows the profile of the core along with radiation (μR/h) readings and uranium solid phase concentrations for the individual drill core sections. The most elevated μR/h readings are in Sample 4 (195 μR/h) and Sample 8B (47 μR/h), which coincide with the highest solid-phase uranium concentrations measured using whole rock chemical analyses shown in Table 1 and Fig. A3. Heterogeneous distribution of uranium throughout the core plays an important role in interpreting the residual mineral and elemental composition, as well as interpretation of the composite sample.

Post-mining measured uranium concentrations (Table 1, Fig. A3) were highly variable in the sampled core intervals and ranged from 5 ppm to 1920 ppm U, with a concentration of 754 ppm U in the composite sample. Pre-mining reserve estimates of the amount of uranium present in mine units were made using gamma logs, and final recoveries of uranium are typically on the order of 80% of these reserve estimates. The maximum uranium concentration was found in Sample 4 (1920 ppm U) at a depth of 235.31–235.46 m below ground surface (bgs), followed by Samples 5 and 8B (both 132 ppm U) at depths of 235.61–235.92 m and 237.29–237.44 m bgs, respectively (Fig. A3). Samples 4 and 8B differed by only a factor of 4 in gamma-ray intensity but differed by a factor of 14.5 in uranium content. This suggests that leached ores were generally U-poor compared to radioactive daughter products, as expected for post-mining core samples because the decay products of uranium composed of radio-isotopes of bismuth, lead, and polonium (Friedlander et al., 1955) are unlikely to be as soluble as uranium in the mildly alkaline lixiviant (leach) solution. However, general radioactive disequilibrium in bulk does not rule out the possible contribution of some unleached primary ore that may more closely approach radioactive equilibrium.

3.3. Uranium oxidation state

The spectroscopic evidence (XANES) showed that residual uranium was present as both U(IV) and U(VI) (Fig. 1). Spectroscopic data also showed that the U(VI)/U(IV) ratio varied considerably between samples. Sample 4 with the largest uranium concentration (1920 ppm U) had an average of 46% U(VI) and 54% U(IV), whereas Sample 8B (132 ppm U) contained 81% U(VI) and 19% U(IV). A linear combination fitting of XANES spectra of the composite sample indicated a mixed valence state of 54% U(VI) and 46% U(IV). The uranium in the composite sample is dominated by contributions from Sample 4, consistent with Table 1.

3.4. Leachable uranium

Although the solid-phase analysis confirmed the presence of residual uranium, post-mining impact to groundwater quality depends on the amount of residual uranium that was accessible and soluble under ambient conditions. A greater amount of uranium was dissolved when the composite sample was leached with deoinized water in the presence of H_2O_2 (1132 μg/L U) or O_2 (1097 μg/L) compared to anoxic deoinized water (543 μg/L U) or anoxic artificial groundwater (406 μg U/L) (Fig. 2). As such, the dissolved uranium concentrations in variably oxic leachates of the composite sample indicated that the total amount of uranium dissolved increased with the oxidizing capacity of the leach solution.

Deionized water leachate in equilibrium with the composite sample had a pH of 7.63 (Table B5), which was within the pH range of 7.5–8.0 measured in groundwater prior to mining. Following addition of H_2O_2 (initial pH = 5.4) to the leachate, the pH decreased

Table 1
Whole rock concentrations of uranium and selected trace elements and μR/h measurements as a function of depth in one-foot sections of the Smith Ranch-Highland drill core extracted from Mine Unit 4. Whole rock composition of major elements can be found in Table B4 in the supplemental information.

Section#	Depth		Rad.	Whole rock composition (ppm)						
	Feet	Meters	μR/h	As	Ni	Pb	Th	U	V	Cr
1	759–760	231.34–231.65	13	4	18	16	6	8	54	40
2	763–764	232.56–232.87	17–19	12	9	18	10	50	63	19
3	765–766	233.17–233.48	16–18	29	13	17	12	78	81	40
4	772–772.5	235.31–235.46	190–200	27	8	17	8	1920	30	13
5	773–774	235.61–235.92	20–22	8	8	20	37	132	27	22
6	776–776.5	236.52–236.68	25–27	4	18	16	10	16	65	51
7	777–778	236.83–237.13	34–37	4	50	22	17	20	123	91
8A	778–778.5	237.13–237.29	45–50	4	26	21	15	78	80	73
8B	778.5–779	237.29–237.44	45–50	3	14	14	10	132	62	36
9	784–785	238.96–239.27	14–15	4	5	10	5	5	33	13
10	786–787	239.58–239.88	18–20	8	8	17	23	129	102	21
Composite	759–787	231.34–239.88	–	16	8	16	9	754	41	18

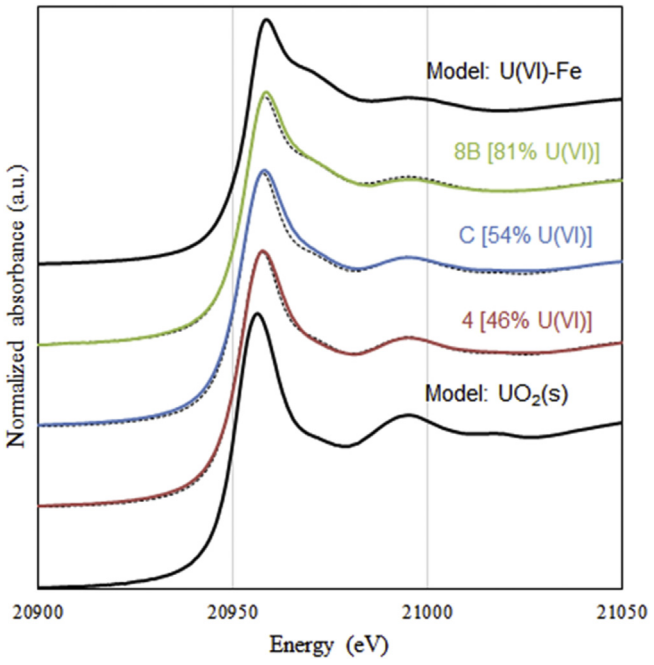

Fig. 1. XANES data (solid lines) and fits (dotted lines) for Sample 8B, homogenized composite (C) of all permeable strata, and Sample 4. The model compounds used for the linear combination fitting were uraninite (100% U(IV)) and U(VI) adsorbed on ferrihydrite. The error on these fits was ± 10%.

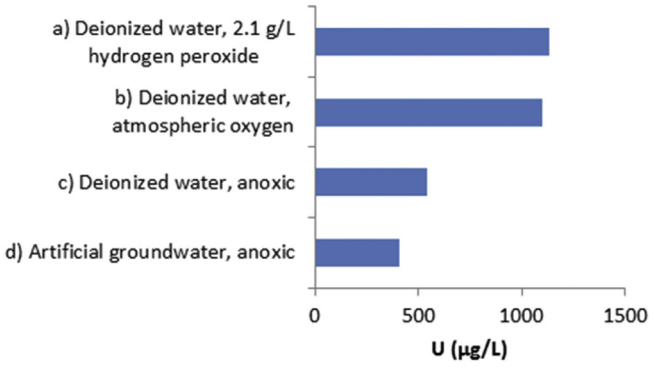

Fig. 2. Uranium concentrations following leaching of the composite sample with various solutions: a) deionized water with hydrogen peroxide; b) deionized water equilibrated with atmospheric O_2(g); c) anoxic deionized water; and d) anoxic artificial groundwater.

to 6.82, which was comparable to the pH of 6.47 in groundwater following ISR mining. The individual samples comprising the composite sample, however, differed in their equilibrated pH after addition of H_2O_2. For example, after addition of H_2O_2 the pH of Sample 4 aqueous leachate increased from 6.9 to 7.4 and uranium concentrations increased from 782 μg/L to 2850 μg/L. Conversely, the pH of Sample 8B leachate decreased from 9.4 to 8.7 and uranium concentrations declined from 411 μg/L U to 181 μg/L U. Additional data on solution compositions are needed to better understand the controlling reactions. In any case, the different pH values reported above for Samples 4 and 8B impacted the stabilities of uranium in residual minerals.

Comparison of the deionized water-soluble fractions versus H_2O_2-extractable fractions of individual samples 8B and 4 (Fig. 3) provided insight into possible mineral hosts. For example, Sample 4, containing the highest concentration of solid phase uranium (1920 ppm U), had the greatest amount of H_2O_2-extractable uranium (2850 μg/L U), and contained about 16 times the H_2O_2-extracted uranium concentration of Sample 8B (181 μg/L U).

The proportions of H_2O_2-leached concentrations of uranium (that is, the actual amounts of leached uranium relative to the total amount of uranium in the sample), however, were comparable in Samples 4 and 8B. About 0.74% and 0.68% of the total uranium present in the solid-phase was leached from Samples 4 and 8B, respectively, when exposed to 2.1 g/L H_2O_2. On the other hand, a much lower proportion of uranium, about 0.20%, was leached with

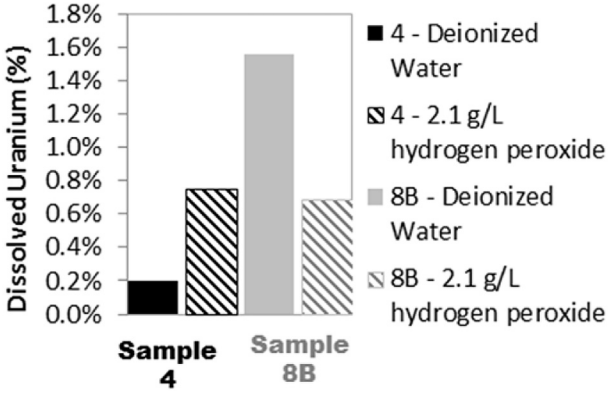

Fig. 3. Oxic leaching of Samples 4 and 8B in deionized water equilibrated with atmospheric oxygen (DI) and deionized water equilibrated with 2.1 g/L hydrogen peroxide (H_2O_2).

deionized water from Sample 4 (which contains 1920 ppm U in the solid phase) than from Sample 8B (1.6%) of lower uranium content (132 ppm U). As such, Sample 8B contained a greater percentage of labile, water-soluble uranium than Sample 4 suggesting that in Sample 8B, phases other than uranium minerals exerted more control on uranium inventory and mobility and that a greater fraction of contained uranium may have resided on surfaces accessible to pore fluids.

3.5. Uranium occurrences by SEM and fission track radiography

All samples were examined using SEM-EDX but uranium was only detected in Sample 4 using this method (detection >1000 ppm U). Fission track radiography was conducted on select samples to provide insight into the distribution of very low to moderate concentrations of uranium that were below SEM-EDX detection limits. Results presented below were categorized as a function of postulated occurrences of rare, relict ore-grade uranium and more common uranium associations with minerals including matrix minerals, organic carbon, or pyrite.

3.5.1. Ubiquitous matrix material

Fission track radiography of a polished thin section of intact Sample 3 (Fig. 4A–C) containing a total of 78 ppm U revealed various mineral hosts of uranium, broadly grouped depending on fission track density as: (1) very low uranium (<5 ppm U) found in quartz, feldspars, calcite; (2) low uranium (5 ppm – low 10s of ppm U) found in chert, magnetite, hornblende, secondary iron oxides; and (3) moderate uranium (several 10s of ppm U) found in apatite, epidote, secondary silica in matrix, mixtures of indeterminate clay-sized materials in inter-granular matrix. A fission track image of a grain mount of the composite sample (754 ppm U by whole rock analyses) (Fig. 4D) showed very low concentrations of uranium occurring as grain coatings that were identified as adhering inter-granular matrix material, which cannot be definitively characterized because it is too fine grained. It is likely that the fine-grained material contains clay minerals but the elevated uranium concentration may be from other clay-sized components of the matrix. The authigenic minerals and secondary alteration products containing uranium were likely added at some time following crystallization and contrasted with the concentrations of uranium contained in detrital, relatively unaltered, primary rock-forming minerals.

3.5.2. Relict ore grade uranium

The SEM-EDX analysis provided evidence for rare sites containing high uranium concentrations in the uranium-rich Sample 4 (1920 ppm U by whole rock analysis). Fig. 5A shows high uranium concentrations (>1000 ppm) in Sample 4 that were associated with clusters of randomly ordered, thin, platy, rectangular crystals (~5 μm edges) containing U, P, Si, Ca, and C located along fractures in host quartz. Although samples were carbon coated prior to SEM analysis, the sizes of the carbon peaks (C) reflected on the EDX spectra are different intensities for each location on the Sample 4 (Fig. 5B, D and F), suggesting that at least part of the contribution to the C peak is due to the presence of carbon in the sample rather than an artifact of the carbon coating. The morphology and chemistry of the U-rich cluster containing P and Ca were consistent with both U-enriched apatite ($Ca_{10}(PO_4)_6(OH)_2$) and autunite ($Ca(UO_2)_2(PO_4)_2 \cdot 10H_2O$). Although U(VI) uptake by surface complexation can occur on apatite surfaces, the concentration of adsorbed uranium would not be detectable by SEM. Apatite may also structurally incorporate uranium in a mixed oxidation state depending on the degree of alteration, with U^{+4} ion substituting for calcium in the apatite structure, which may subsequently oxidize to U(VI) (Altschuler et al., 1958). The fact that the uranium was observed using SEM suggests higher concentrations (~>1000 ppm U), which were not feasible loadings on apatite. Therefore, uranium was likely present as a solid-solution (not adsorbed) or as individual uranium minerals. Fig. 5C,D shows a particle from a panned fraction from Sample 4 (Fig. A4) with elevated U/O with minor Ca and Si and C. Fig. 5E,F also shows a particle containing elevated U/O/Si and embedded high Fe/S particles, thought to be pyrite in the vicinity of C, potassium-feldspar (k-feldspar) and chlorite. These high concentrations of uranium and associated elements were consistent with both coffinite ($U(SiO_4)_{1-x}(OH)_{4x}$), and uraninite (UO_2), which were thought to comprise uranium deposits at Smith Ranch-Highland (Stewart et al., 2000).

3.5.3. Organic carbon

Samples 2, 3 and 8A, which contained relatively high concentrations of organic C (1.14–1.62%), were host to low concentrations of U (50–78 ppm U) measured by whole rock analysis (Table B4). In contrast to bulk measurements, fission track radiography of larger fragments of organic matter within uranium-rich Sample 4 indicated consistent association of carbonaceous material (Fig. 6A) with homogeneous fission track density, i.e., uranium concentration (Fig. 6B). The concentration of uranium in organic matter was qualitatively estimated as greater than several 10 s ppm U based on fission track densities.

3.5.4. Unaltered framboidal pyrite

Framboidal pyrite was thought to be the product of bacterially-mediated sulfate reduction during early diagenesis. Such fine-grained pyrite was unlikely to have survived during transport of organic detritus in surficial streams and was more likely an early product of diagenesis once the organic-bearing sediments were deposited and buried. The scanning electron and transmitted light microscopic images of Sample 3 (Fig. 6C–E) indicate that framboidal pyrite occurs along fractures within the organic matter. The pyrite framboids (Fig. 6D) showed minimal corrosion suggesting that they were not affected by leaching (lixiviant) solutions. Furthermore, the absence of elevated fission-track densities along the fractures (Fig. 6F) indicated that uranium was not found in association with framboidal pyrite.

3.5.5. Weathered euhedral pyrite

In addition to fine-grained framboidal pyrite, the host rocks contained coarser-grained euhedral pyrite shown in the electron microprobe and SEM imaging of Sample 8B (Fig. 7A–C). Uranium concentrations near these euhedral pyrites were below the detection limit of the SEM-EDX and electron microprobe analyses. Fission track radiographs showed that most of these larger pyrites did not contain uranium in their interior (Fig. 7D), but rather on the weathered euhedral pyrite surfaces. Some of the occurrences of euhedral pyrite had irregular distributions of moderate to high nearby associated concentrations of uranium (detectable only by fission track radiography, Fig. 7D). Comparison of Fig. 7C–E revealed that fission track density was also elevated either at the interface between chlorite and elongated pyrite inclusions or exclusively on the surfaces of chlorite or altered euhedral pyrite. In both cases, electron microprobe images (Fig. 7A,B) indicated that these areas of elevated uranium were sulfur-poor and iron-rich compared to pyrite and iron-rich compared to nearby inter-granular matrix of lesser uranium content.

When highly oxidizing leach solution containing H_2O_2 interacted with Sample 8B there was a drop in pH from pH 9.4 to 8.7 (Table B5). This is consistent with oxidation of ferrous to ferric iron and the formation of hydrous iron oxides, which are known to sorb uranium from solution. A SEM image of Sample 8B (Fig. 7F)

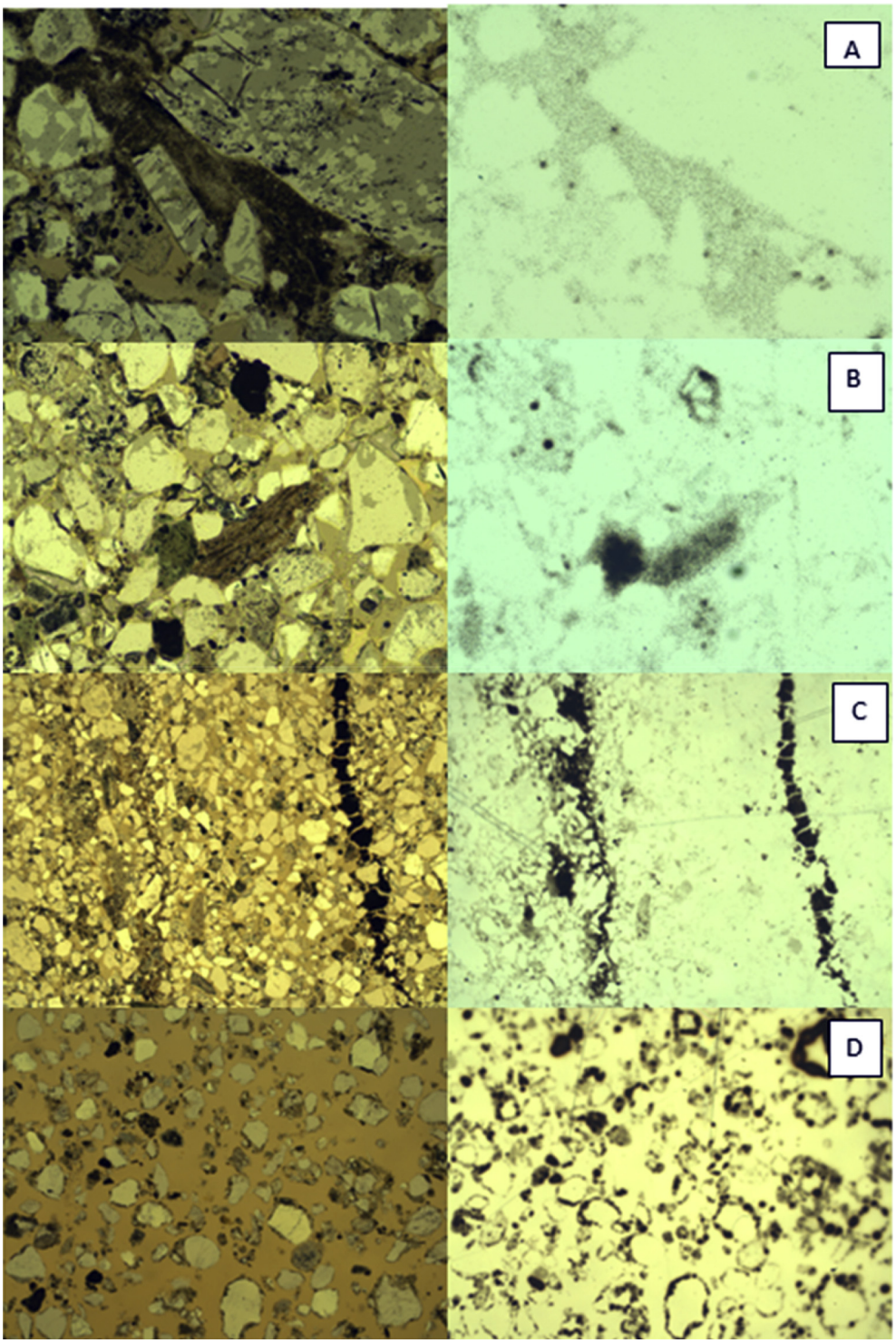

Fig. 4. Selected photomicrographs of thin sections (left) and corresponding fission track radiographs (right) indicating the location and distribution of U. Areas of highest fission track density (and U content) appear as dark areas in the radiographs. (A) Fine grained inter-granular matrix of moderate U content contrasts with coarse detrital silicate grains of very low U content (Sample 3, horizontal dimension 1.15 mm). (B) Detrital grains of variably altered mafic minerals show moderate U content compared to nearby matrix (low U) and detrital silicates of very low U (Sample 3, horizontal dimension 1.15 mm). (C) Thin vertical stringer of dark opaque organic matter (right) and sub-parallel zone of fine grained inter-granular matrix, both of moderate to high U content (Sample 3, horizontal dimension 1.15 mm). (D) grain mount from composite sample shows U rims (dark areas) that were low to moderate in U content and mostly composed of fine-grained matrix that remains attached to grain surfaces (horizontal dimension 4.6 mm).

illustrates that some Fe–S-bearing grains had an irregular dendritic surface texture that could indicate partial dissolution of a pyrite grain under oxidizing conditions imposed by ISR and subsequent groundwater restoration.

3.6. Microbial consortia in leached ore

Aside from possible abiotic controls on redox state, microorganisms may also play a role in poising redox conditions. Fig. 8

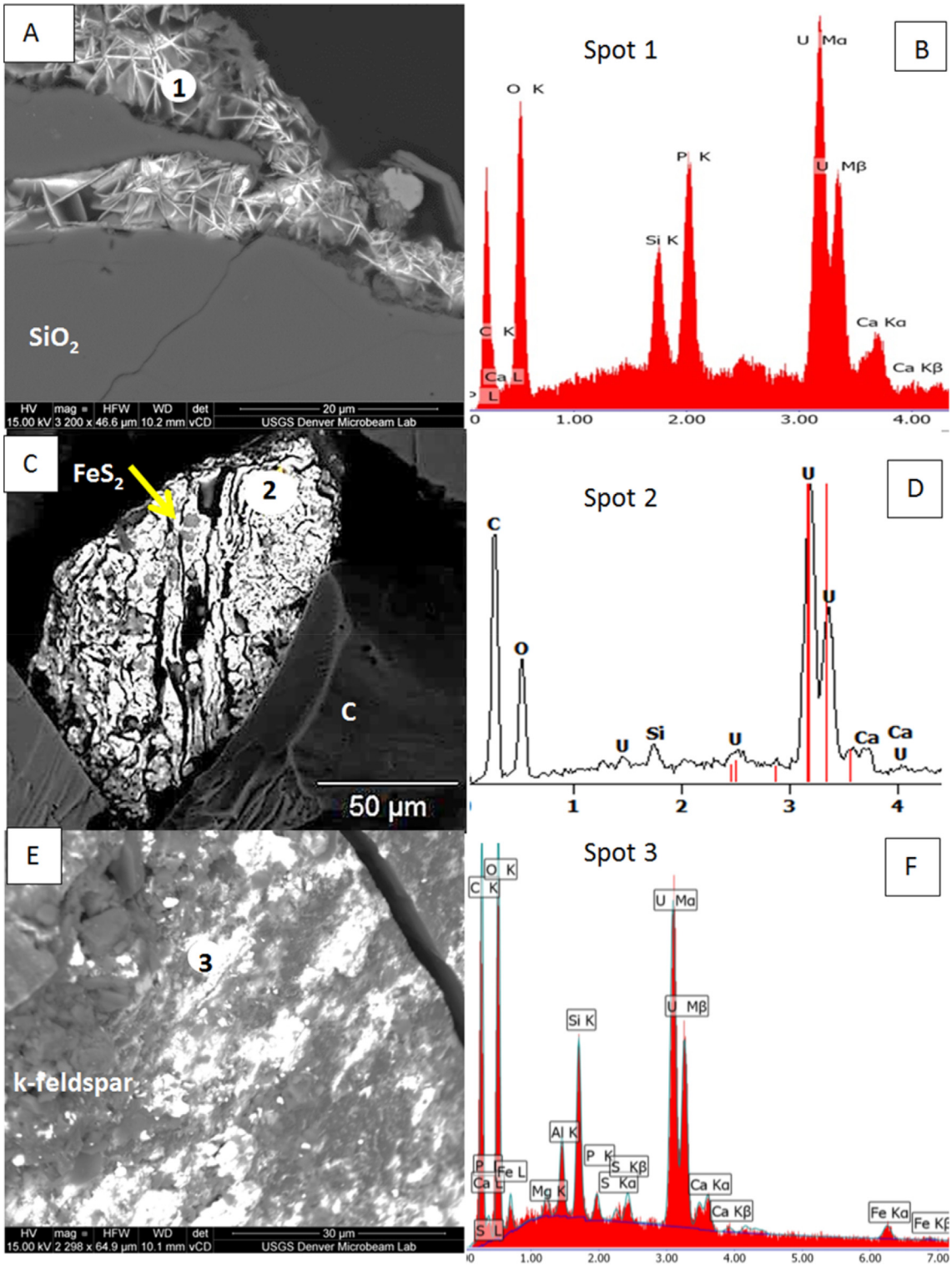

Fig. 5. Sample 4: (A) SEM BSE (200×) of bright crystals of a uranium-rich mineral residing in fractures of SiO_2 and (B) the corresponding EDX of spot (1) indicating the presence of U and Ca/P. (C) SEM BSE (700×) showing bright areas indicating uranium particle and (D) the corresponding EDX of spot (2) showing bright areas consist mainly U/O on C with minor amounts of Ca and embedded FeS_2 particles. (E) SEM BSE (2300×) showing small patches containing uranium and (F) the corresponding EDX of spot (3) indicating that uranium mineral contains U/O on carbon and k-feldspar with minor amounts of Ca, pyrite and chlorite.

indicates the composition and alpha diversity of the microbial population in the sampled core intervals. Microbial community analysis measures the amount and identity of bacteria present but not necessarily the activity of the taxonomic groups. The identity of organisms present in the core samples, however, can be used to hypothesize metabolism based on relatedness to known, cultured organisms. Members of the microbial community in the drill core samples were phylogenetically diverse (beta diversity, Tables B6-7).

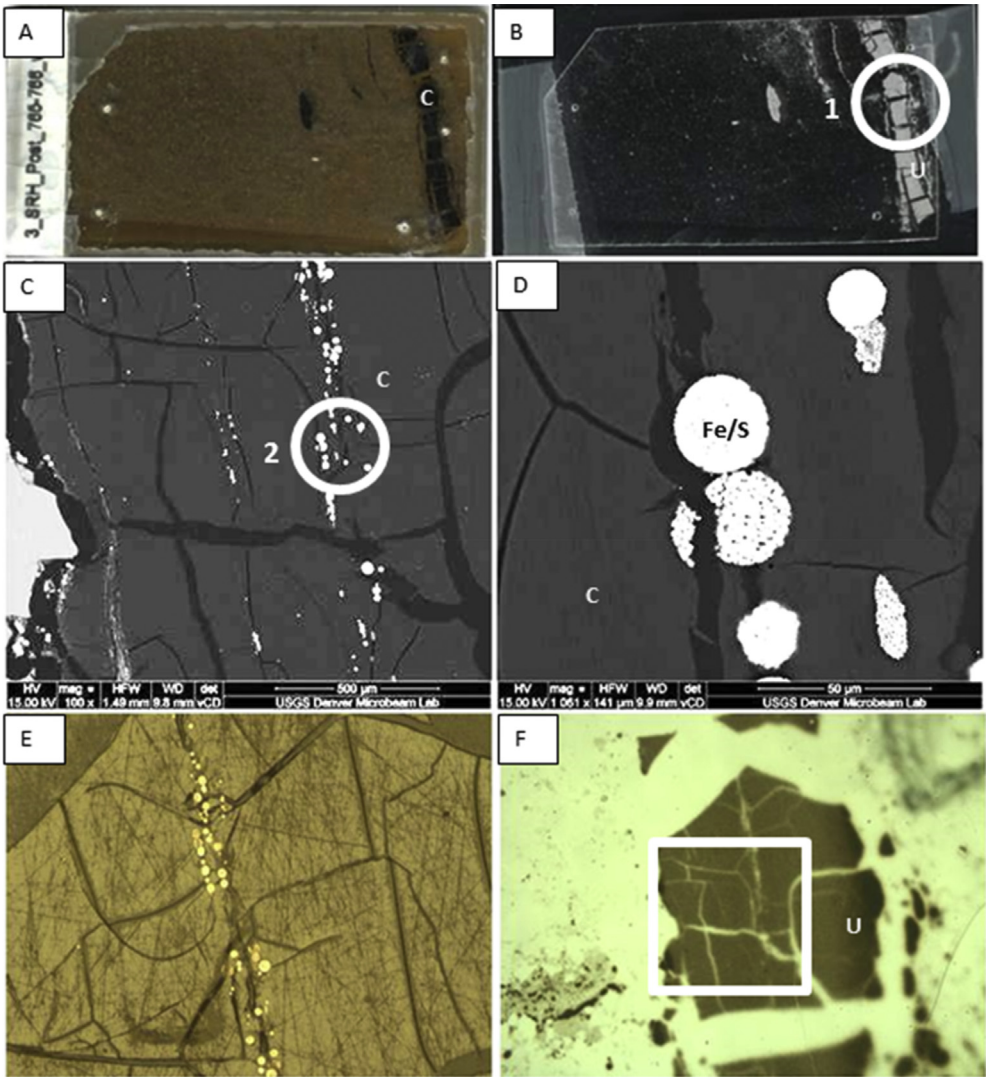

Fig. 6. Sample 3: (A) transmitted light image of a polished thin section with dark areas indicating organic C-rich material; (B) fission track radiograph of (A) under reflected light illumination with bright areas indicating areas of highest U concentration; (C) SEM BSE with bright areas indicating Fe and S, in the magnified area (100×) corresponding to area (1) in (B); (D) SEM BSE (1061×) showing framboidal pyrite clusters along fractures in the host organic matter corresponding to area (2) in (C); (E) reflected light image with bright spots, corresponding to locations of framboidal pyrite in (C); and (F) fission track image (with area inside box closely corresponding to (C)) shows that darker areas reflecting higher uranium concentrations are absent along fractures.

There were no significant trends in overall community with depth, mineralogy, or elemental composition. In this system, control over the community composition and diversity was likely a combination of factors, such as permeability, local redox state, as well as elemental composition, but additional data are needed to constrain the important influences. Even without a clear connection to geochemical and mineralogical parameters measured in this study, the taxonomy of the community provided insight into potentially important processes. Many of the dominant bacteria were those commonly found in soils and other types of uranium ore deposits (e.g., *Holophagales*, *Staphylococcus*, *Burkholdaria*, *Ralstonia*) (Islam et al., 2011; Mondani et al., 2011). Many of the abundant bacteria identified have the ability to degrade organic carbon, especially recalcitrant forms of organic matter, which were likely present in the ore zone. Although the composition of the organic carbon found at the site has not been characterized, in the Shirley Basin (WY), the roll front deposit contains coalified woody material (Granger and Warren, 1969). The organic material at Smith Ranch-Highland may be similar, and could serve as an electron donor for microbial activity.

The rare organisms (defined here to be <10% of the total sequences for a given sample) showed a wide range of putative metabolisms and suggested that a variety of redox microenvironments existed in the samples, consistent with the mineralogical data. A number of Fe- and S-oxidizing organisms were present, such as *Acidithiobacillus*, *Thiobacillus*, *Sideroxydans*, and *Leptothrix*. Interestingly, *Acidithiobacillus* are acidophilic (pH < 4) Fe-oxidizing organisms, while *Leptothrix* and *Sideroxydans* are neutrophilic Fe-oxidizing organisms, indicating strong pH gradients (e.g., around pyrite grains). *Sideroxydans* is also known to thrive at oxic/anoxic boundaries. Additionally, evidence of competing redox processes in the community data, such as the presence of both sulfate-reducing organisms (*Desulfovibrio*) along with Fe-oxidizing organisms (*Leptothrix*), was found in the same sample (Sample 3). Similarly, strict anaerobic organisms co-occurred with strict aerobes, providing additional evidence for the importance of microenvironments in determining the bacteria that thrive and potentially control important redox processes. The high level of phylogenetic and metabolic diversity suggests microbial flexibility and adaptability within the aquifer as redox and geochemical conditions change.

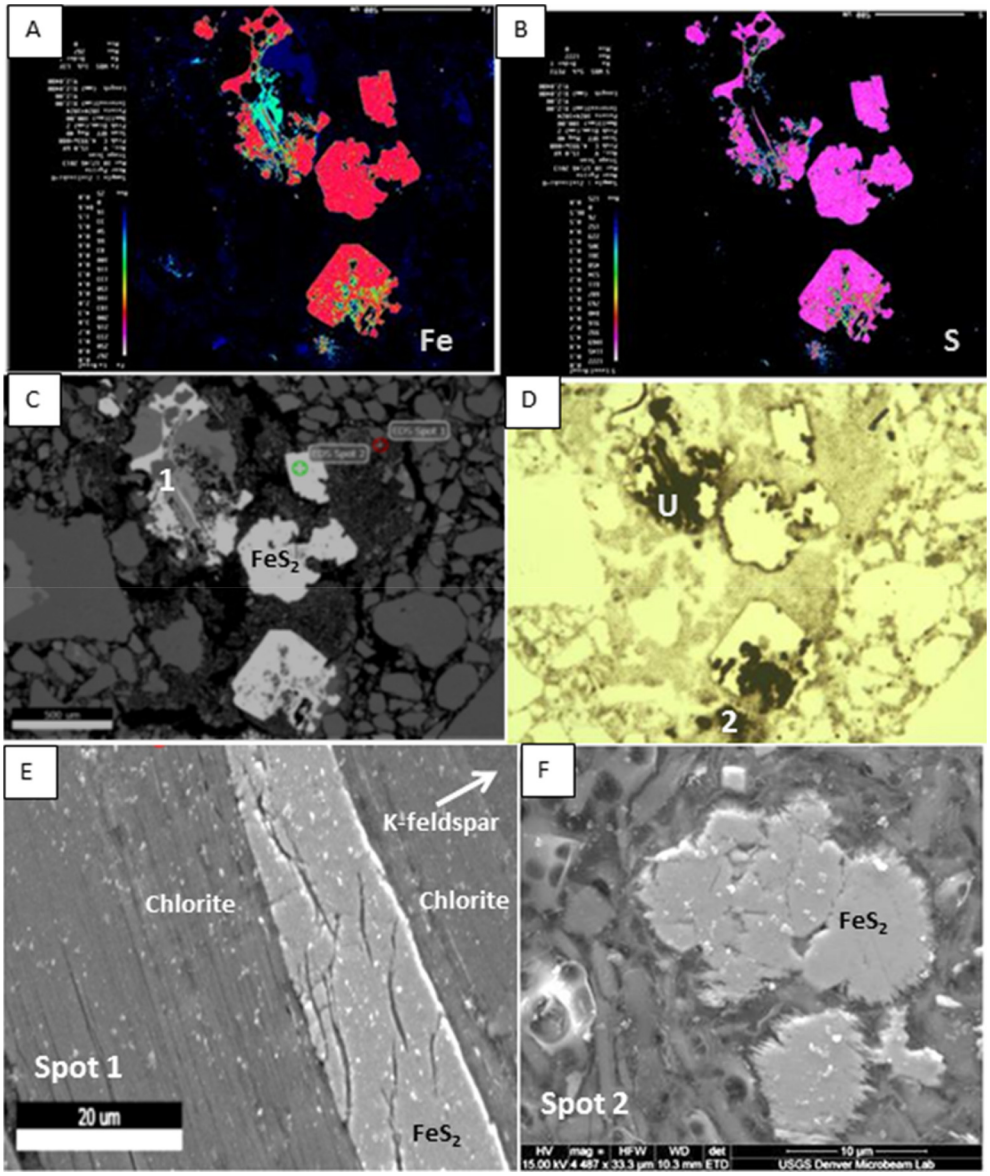

Fig. 7. Sample 8B: Microprobe analysis showing elemental maps of (A) Fe and (B) S concentrations and corresponding (C) SEM BSE image and (D) fission-track radiograph, where darker areas of higher fission track density reveal U-rich areas. (E) Spot 1: SEM BSE image showing an elongated pyrite inclusion in chlorite and nearby potassium feldspar. (F) Spot 2: SEM BSE image showing the acicular/dendritic surface morphology of some FeS_2 particles (altered euhedral pyrite) associated with U.

4. Discussion

Following ISR uranium mining, persistent uranium was present as a mixture of both oxidized U(VI) and reduced U(IV). Residual uranium primarily was associated with (1) refractory organic matter found in relatively impermeable inter-granular matrices in some scattered locations, likely as U(IV) minerals (uraninite or coffinite), (2) alteration products of pyrite and/or chlorite including iron oxides, and (3) secondary U(VI) minerals (such as autunite). The organic carbon hosts survived relatively aggressive attack by oxidizing solutions because of their low solubility and/or poor access to leach solutions and were likely to remain relatively recalcitrant sources of uranium in the post-mining period. In contrast, secondary U(VI) that may have formed during ISR mining, including U(VI) sorbed to solution-accessible iron oxides, newly precipitated U-rich coatings, and residual leach solutions containing dissolved U(VI), may provide more accessible labile sources of uranium, depending on evolving redox conditions.

Although the intention of ISR was to dissolve the uranium in the deposit into the groundwater, these data demonstrated that uranium was present in the solid phase following both mining and groundwater restoration. Furthermore, certain horizons within the sampled ore zone were less oxidized than others (e.g., Sample 4), contrary to the assumption that U was mostly oxidized following ISR mining and groundwater restoration. The persistent residual uranium was heterogeneously distributed, especially compared to other chemical constituents (Table 1 and Fig. A1), throughout leached ore or pockets of minimally oxidized primary ore.

Uranium minerals such as autunite, coffinite and/or uraninite persisted likely because the lixiviant failed to contact impermeable areas of the subsurface where these minerals were found (WoldeGabriel et al., 2014). It was also probable that variably efficient solution mining, including variability in contact of the lixiviant solution with different portions of the ore zone, introduced additional heterogeneity in bulk chemistry and mineralogy. Spatial association of U-rich particles with C indicated possible locally

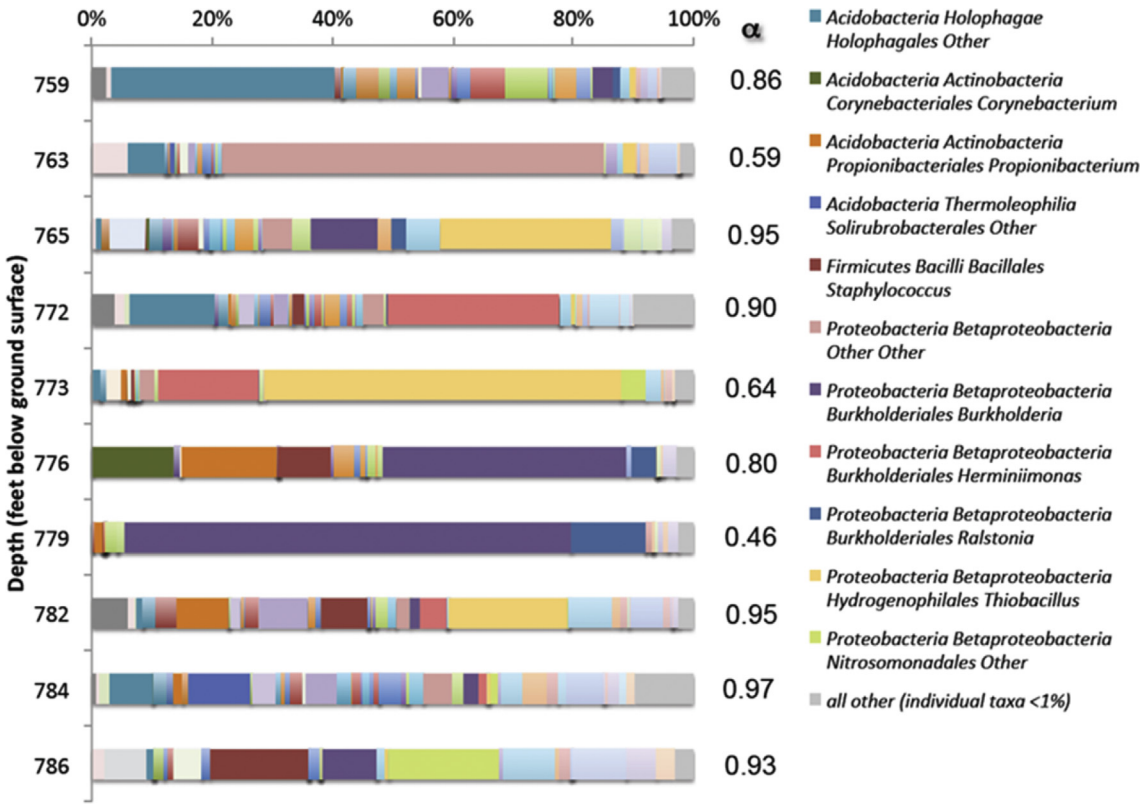

Fig. 8. Microbial Community (16S rRNA) analysis results. Taxonomy was assigned to the genus level. Each color block in this figure represents a unique group (genus) for all taxa present at greater than 1% of the total sequences for each sample. Taxa that comprise at least 10% of the total sequences for each sample were identified in the legend, and a complete list of the taxa identities were presented in Table B6. Alpha diversity was quantified using the Simpson metric, denoted on the figure as "α". Visually, more color blocks indicate a higher alpha diversity, which was quantified in the alpha metric (higher alpha indicates higher diversity).

reducing conditions and provided evidence of unoxidized relict ore-grade materials retained by organic matter; microbial populations capable of utilizing organic carbon may contribute to these locally reducing conditions. Furthermore, bypassed regions of the subsurface that were accessible primarily only by diffusion may have been critically important in the persistence of reduced phases like organic carbon and pyrite. Pyrite has been cited as a reductant of U(VI) (Descostes et al., 2010; Eglizaud et al., 2006; Wersin et al., 1994). Survival of very fine-grained framboidal pyrite within the organic carbon after solution mining indicated that some areas of the drill core were less affected by the oxidizing leaching solutions circulated during mining. However, these rare individual framboids suspended in the fine-grained inter-granular matrix showed little evidence of uranium enrichment in their immediate vicinity.

Although uranium was not particularly concentrated in areas of framboidal pyrite, uranium-enriched areas of euhedral pyrite grains were evident. U(VI) sorbed on pyrite was possible via partial reduction of uranium to form UO_{2+x} (s) and in some cases, in close association with oxidized sulfur and iron oxyhydroxide reaction products (Descostes et al., 2010; Eglizaud et al., 2006; Wersin et al., 1994). Because uranium was not found on all euhedral pyrite surfaces, but rather in isolated, weathered, Fe-rich/S-poor areas of euhedral pyrite surfaces or associated weathered chlorite surfaces, the most likely hosts of the low concentrations of uranium were secondary iron oxides. During both euhedral pyrite and/or chlorite weathering, the formation of coatings of iron oxides was likely (Krawczyk-Bärsch et al., 2004; Waite et al., 1994). U(VI) can be incorporated into or co-precipitated with iron oxides (Duff et al., 2002; Nico et al., 2009; Stewart et al., 2009) or uranyl can sorb onto iron oxides (Waite et al., 1994) as either a uranyl-carbonato or uranyl-calcium carbonato inner sphere complex (Bargar et al., 1999) or uranyl surface complex (Hiemstra et al., 2009). As such, uranyl (i.e., U(VI)) could sorb on either weathered pyrite or chlorite surfaces and/or surfaces of ferrihydrite coatings or colloids formed during chlorite and pyrite dissolution (Krawczyk-Barsch, 2012; Waite et al., 1994). Uranium has been shown to be sorbed directly onto chlorite surfaces as an inner sphere complex, with loadings up to 6.3 μmol U/g chlorite with greatest sorption in CO_3—Ca bearing systems (Singer et al., 2009). As such, weathered pyrite and chlorite surfaces and iron oxide surfaces can be an important sink for U(VI) in the Smith Ranch-Highland samples.

Oxidation of pyrite may have been caused by direct oxidation via the lixiviant, or indirectly through the stimulation of Fe- and S-oxidizing bacteria with the introduction of dissolved oxygen. Evidence of acidophilic pyrite oxidizing organisms, such as *Acidithiobacillus*, was found in the 16S rRNA community analysis, and they could have played an important role in oxidation of pyrite and precipitation of secondary iron minerals. Such alteration could have preceded ISR mining in which case uranium enrichment was a preserved feature of the original reduced ore deposit. Alternatively, uranium enrichment could have been related to ISR mining, possibly on mixed ferrous and ferric oxides, as the result of sorptive uptake from uranium-rich oxidizing pore-fluids.

Sample 8B contained relatively little reduced U(IV) (19%), so addition of an oxidizing agent had less effect on uranium concentrations than for Sample 4, which contained approximately 54% U(IV). Sample 8B (132 ppm U), however, contained relatively little mineralized uranium and a greater percentage of labile, water-soluble uranium so the assemblage of uranium-host phases were very different than the relict uranium minerals identified in Sample

4. The comparative leachability of U(IV)-rich Sample 4 and U(IV)-poor Sample 8B in deionized water amended with O_2 and H_2O_2 suggested that (1) under highly oxic conditions the concentration of dissolved uranium in pore waters of relict ore could be influenced by continued aggressive oxidation of remaining reduced U(IV) and (2) under less oxidizing conditions closer to natural pre-mining conditions, dissolved uranium included greater relative contributions of the more soluble, previously oxidized U(VI). Furthermore, the much higher pH of the deionized water after contact with Sample 8B should have promoted both a higher solubility of U(VI) phases and greater desorption of U(VI). The higher pH suggested the presence of a small amount of calcite in 8B (below detection by XRD), or possibly a pH buffering effect controlled by clays such as smectite. The higher pH and increase in carbonate/bicarbonate content to the deionized water could have resulted in more efficient leaching of uranium. It was possible that much of the U(VI) was adsorbed onto surfaces, such as iron oxides, and desorption was an important control on release of U(VI) into water.

5. Conclusions

Taken together, the leaching results and solid phase analyses demonstrated that the permeable strata contained soluble and labile fractions of uranium, likely sorbed as U(VI), and the less permeable strata contained residual oxidizable U(IV). Because uranium residing on grain coatings (as sorbed phases) or intergranular matrix may be more easily accessed by groundwater (as opposed to uranium incorporated within insoluble primary and secondary minerals), labile phases, namely U(VI) sorbed onto iron oxide surfaces, can remain a source of uranium following recovery and restoration if native reducing groundwater re-equilibrates with solids in the mining zone.

The presence of U(VI) sorbed onto ferric iron oxides that are formed during ISR-mining may present a special restoration challenge, as the re-establishment of reducing conditions could cause conversion of ferric solids to more soluble ferrous iron, thus resulting in dissolution of the solids and liberation of the sorbed U(VI) (Anastasi et al., 1985). The persistence of such labile uranium-rich sources coupled with the local redox poising provided by iron sulfides and organic carbon persisting after mining may help explain short-term "rebounding" of uranium concentrations following groundwater restoration that occurs at some ISR sites.

In the longer term, however, reductants including residual pyrite and organic carbon as well as metal-reducing bacteria could assist in establishing and maintaining low concentrations of redox-sensitive constituents such as uranium through reductive precipitation after restoration. Although the likely controls on residual uranium mobility after ISR mining depend on the uranium-host minerals and microbial and abiotic controls on redox, the abundance of organic carbon and pyrite in the leached, now oxidized, ore zones may or may not be sufficient to re-establish reducing conditions on the scale needed to stabilize any remaining uranium within the mining zone. Microbially induced reducing conditions may be possible, but are dependent upon the availability and lability of electron donors in the aquifer. Stimulation of the microbial community may be necessary. The role of microorganisms in establishing reducing conditions (e.g., reductive dissolution of iron oxides) and driving redox changes *in situ* needs to be assessed with additional data.

The Eh and pH are master variables that will influence the solubility of solids and sorption efficiency and thus the mobility of uranium and other trace elements within and down gradient of the mining zone. Future studies could monitor changes in redox conditions in the mining zone as a result of introduced reductants or re-equilibration with in-situ reductants. Although measurement of redox potential and concentrations of redox couples such as Fe(III)/Fe(II) and SO_4^{2-}/S^{2-} can be challenging, they are required to better understand the redox ladder for the aquifer being restored as the water chemistry evolves from interaction with minerals that persist following uranium ISR and restoration.

Acknowledgments

Financial support for this research was provided by Energy Resources Program, the Toxic Substance Hydrology Program, and the National Research Program at the U.S. Geological Survey. Thanks to collaborators at Cameco/Power Resources for providing access to drill core and water quality information especially Larry Reimann, Christopher Stanbury and Katelynd Faler. Whole rock digests and XRD were performed at the USGS Crustal Geochemical Labs in Denver, CO. Thanks to Heather Lowers for assistance with SEM and EMP analyses. X-ray absorption was performed at the Stanford Synchrotron Radiation Lightsource, a facility operated by the Department of Energy Office of Basic Energy Sciences. Funding for Janot and Bargar was provided by the DOE Office of Biological and Environmental Research, Subsurface Biogeochemistry Research (SBR) program via the SLAC SFA program, under contract DE-AC02-76SF00515. Any use of trade, firm, or product names was for descriptive purposes only and does not imply endorsement by the U.S. Government. Neither the United States Government nor any agency thereof, nor any of its employees, make any warranty, expressed or implied, or assume any legal liability or responsibility for the accuracy, completeness, or usefulness of any information, apparatus, product, or process disclosed in this article, or represent that its use would not infringe privately owned rights.

Appendix A. Supplementary information

Supplementary information related to this article can be found at http://dx.doi.org/10.1016/j.apgeochem.2015.08.017.

References

Altschuler, Z.S., Clarke Jr., R.S., Young, E.J., 1958. The Geochemistry of Uranium in Apatite and Phosphorite. United States Government Printing Office, Washington, D.C. U.S. Geological Survey Professional Paper 314-D.

Anastasi, F.S., Williams, R.E., Hancock, S., 1985. Discussion on aquifer restoration at uranium in situ leach sites. Int. J. Mine Water 4 (4), 55–56.

Bargar, J.R., Reitmeyer, R., Davis, J.A., 1999. Spectroscopic confirmation of uranium(VI)-carbonato adsorption complexes on hematite. Environ. Sci. Technol. 33 (14), 2481–2484.

Borch, T., Roche, N., Johnson, T.E., 2012. Determination of contaminant levels and remediation efficacy in groundwater at a former in situ recovery uranium mine. J. Environ. Monit. 14 (7), 1814–1823.

Caporaso, J.G., Kuczynski, J., Stombaugh, J., Bittinger, K., Bushman, F.D., Costello, E.K., Fierer, N., Peña, A.G., Goodrich, J.K., Gordon, J.I., Huttley, G.A., Kelley, S.T., Knights, D., Koenig, J.E., Ley, R.E., Lozupone, C.A., McDonald, D., Muegge, B.D., Pirrung, M., Reeder, J., Sevinsky, J.R., Turnbaugh, P.J., Walters, W.A., Widmann, J., Yatsunenko, T., Zaneveld, J., Knight, R., 2010. QIIME allows analysis of high-throughput community sequencing data. Nat. Methods 7 (1), 2.

Catchpole, G., Kuchelka, R., 16-20 Aug 1993. Groundwater restoration of uranium ISL mines in the United States: paper 10. In: Proceedings workshop on uranium production environmental restoration: an exchange between the United States and Germany. NM1993, IAEA, International Nuclear Information System, Albuquerque, p. 9. Also available from: OSTI as DE94008528; NTIS. Accessed on 8.05.15 at. https://inis.iaea.org/search/search.aspx?orig_q=RN:26025786.

Dahl, A.R., Hagmaier, J.L., 2005. Genesis and characteristics of the southern Powder River Basin uranium deposits, Wyoming, geology and energy resources of the Powder River. In: 28th Annual Field Conference Guidebook, 1976. Wyoming Geological Association, pp. 243–252.

Darling, B.K., 2008. Report on Findings Related to the Restoration of Groundwater at In-situ Uranium Mines in South Texas. Southwest Groundwater Consulting, LLC, Houston, TX. Found at. http://www.powertechexposed.com/BK_Darling%20Report_Complete_Sept_30.pdf (accessed 30.07.15.).

Davis, J.A., Curtis, G.P., 2007. Consideration of Geochemical Issues in Groundwater Restoration at Uranium In-situ Leach Mining Facilities. U.S. Nuclear Regulatory Commission. Division of Fuel, Engineering, and Radiological Research & U.S. Geological Survey. NUREG/CR-6870.

Descostes, M., Schlegel, M.L., Eglizaud, N., Descamps, F., Miserque, F., Simoni, E., 2010. Uptake of uranium and trace elements in pyrite (FeS_2) suspensions. Geochim. Cosmochim. Acta 74 (5), 1551–1562.
Deutsch, W.J., Eary, L.E., Martin, W.J., McLaurine, S.B., 1985. Use of sodium sulfide to restore aquifers subjected to in situ leaching of uranium ore deposits. In: Proceedings Association of Ground Water Scientists and Engineers: Western Regional Ground Water Conference, Reno, NV, pp. 129–153.
Duff, M.C., Coughlin, J.U., Hunter, D.B., 2002. Uranium co-precipitation with iron oxide minerals. Geochim. Cosmochim. Acta 66 (20), 3533–3547.
Eberl, D.D., 2003. User Guide to RockJock – a Program for Determining Quantitative Mineralogy from X-ray Diffraction Data. U.S. Geological Survey Open File Report 2003-78, Boulder, CO, 47.
Eglizaud, N., Miserque, F., Simoni, E., Schlegel, M., Descostes, M., 2006. Uranium(VI) interaction with pyrite (FeS_2). Chem. Spectrosc. Stud. Radiochim. Acta 94 (9–11), 651–656.
Friedlander, G., Kennedy, J.W., Miller, J.M., 1955. Nuclear and Radiochemistry, second ed. John Wiley and Sons, New York, p. 585.
Gallegos, T.J., Fuller, C.C., Webb, S.M., Betterton, W., 2013. Uranium(VI) interactions with mackinawite in the presence and absence of bicarbonate and oxygen. Environ. Sci. Technol. 47 (13), 7357–7364.
Granger, H.C., Warren, C.G., 1969. Unstable sulfur compounds and the origin of roll-type uranium deposits. Econ. Geol. 64 (2), 160–171.
Hall, S., 2009. Groundwater Restoration at Uranium In-situ Recovery Mines, South Texas Coastal Plain. U.S. Geological Survey Open File Report 2009-1143. U.S. Geological Survey, Reston, VA, p. 31.
Hiemstra, T., Riemsdijk, W.H.V., Rossberg, A., Ulrich, K.-U., 2009. A surface structural model for ferrihydrite II: adsorption of uranyl and carbonate. Geochim. Cosmochim. Acta 73 (15), 4437–4451.
Hyun, S.P., Davis, J.A., Sun, K., Hayes, K.F., 2012. Uranium(VI) reduction by iron(II) monosulfide mackinawite. Environ. Sci. Technol. 46 (6), 3369–3376.
IAEA, 2005. Guidebook on Environmental Impact Assessment for in Situ Leach Mining Projects. IAEA-TECDOC-1428. International Atomic Energy Association.
Islam, E., Dhal, P.K., Kazy, S.K., Sar, P., 2011. Molecular analysis of bacterial communities in uranium ores and surrounding soils from Banduhurang open cast uranium mine, India: a comparative study. J. Environ. Sci. Health Part A Toxic/Hazardous Subst. Environ. Eng. 46, 271–280.
Krawczyk-Bärsch, E.A., Arnold, T., Reuther, H., Brandt, F., Bosbach, D., Bernhard, G., 2004. Formation of secondary Fe-oxyhydroxide phases during the dissolution of chlorite – effects on uranium sorption. Appl. Geochem. 19 (9), 1403–1412.
Krawczyk-Bärsch, E.A., 2012. The effect of chlorite dissolution on the sorption behavior of U(VI). In: Merkel, Broder, Planer-Friedrich, B., Wolkersdorfer, Christian (Eds.), Uranium in the Aquatic Environment: Proceedings of the International Conference Uranium Mining and Hydrogeology III and the International Mine Water Association Symposium Freiberg, Germany, 15-21 September 2002 (Google eBook). Springer Science & Business Media, p. 1112.
Langmuir, D., 1979. Chemistry of Uranium in Groundwater: Institution of Mechanical Engineers. Conference Publications, pp. 75–106.
Love, J.D., Christiansen, A.C., 1985. Geologic Map of Wyoming. U.S. Geological Survey, Reston, VA.
Mondani, L., Benzerara, K., Carriere, M., Christen, R., Mamindy-Pajany, Y., Fevrier, L., Marmier, N., Achouak, W., Nardoux, P., Berthomieu, C., Chapon, V., 2011. Influence of uranium on bacterial communities: a comparison of natural uranium-rich soils with controls. PLoS One 6 (10), e25771, 1–11.
Moyes, L.N., Jones, M.J., Reed, W.A., Livens, F.R., Charnock, J.M., Mosselmans, J.F.W., Hennig, C., Vaughan, D.J., Pattrick, R.A.D., 2002. An X-ray absorption spectroscopy study of neptunium(V) reactions with mackinawite (FeS). Environ. Sci. Technol. 36 (2), 179–183.
Moyes, L.N., Parkman, R.H., Charnock, J.M., Vaughan, D.J., Livens, F.R., Hughes, C.R., Braithwaite, A., 2000. Uranium uptake from aqueous solution by interaction with goethite, lepidocrocite, muscovite, and mackinawite: an X-ray absorption spectroscopy study. Environ. Sci. Technol. 34 (6), 1062–1068.
Nico, P.S., Stewart, B.D., Fendorf, S., 2009. Incorporation of oxidized uranium into Fe (hydr)oxides during Fe(II) catalyzed remineralization. Environ. Sci. Technol. 43 (19), 7391–7396.
Power Resources Inc., 2004. Smith Ranch–Highland Uranium Project, A-wellfield Groundwater Restoration Information. Glenrock, Wyoming.
Quast, C., Pruesse, E., Yilmaz, P., Gerken, J., Schweer, T., Yarza, P., Peplies, J., Glöckner, F.O., 2013. The SILVA ribosomal RNA gene database project: improved data processing and web-based tools. Nucl. Acids Res. 41 (D1), D590–D596.
Ravel, B., Newville, M., 2005. Athena, artemis, hephaestus: data analysis for X-ray absorption spectroscopy using IFEFFIT. J. Synchrotron Radiat. 12, 537–541.
Santos, E.S., Ludwig, K.R., 1983. Age of uranium mineralization at the Highland Mine, Powder River Basin, Wyoming, as indicated by U-Pb isotope analyses. Econ. Geol. 78, 498–501.
Singer, D.M., Maher, K., Brown Jr., G.E., 2009. Uranyl–chlorite sorption/desorption: evaluation of different U(VI) sequestration processes. Geochim. Cosmochim. Acta 73 (20), 5989–6007.
Stewart, B.D., Nico, P.S., Fendorf, S., 2009. Stability of uranium incorporated into Fe (hydr)oxides under fluctuating redox conditions. Environ. Sci. Technol. 43 (13), 4922–4927.
Stewart, C.L., Reimann, L.J., Swapp, S.M., 2000. Mineralogic considerations for uranium in situ leach mining: a preliminary study of uranium and associated mineralogy of roll-front uranium deposits in Wyoming and Nebraska. Cim. Bull. 93 (1045), 89–96.
Vogt, T.C., Strom, E.T., Venuto, P.B., Winget, J.E., Scoggins, M.W., 1984. In-situ leaching of Crownpoint, New Mexico, uranium ore: part 6-section 9 pilot test. J. Pet. Technol. 36 (12), 2243–2254.
Waite, T.D., Davis, J.A., Payne, T.E., Waychunas, G.A., Xu, N., 1994. Uranium(VI) adsorption to ferrihydrite: application of a surface complexation model. Geochim. Cosmochim. Acta 58 (24), 5465–5478.
Wersin, P., Hochella, M.F., Persson, P., Redden, G., Leckie, J.O., Harris, D.W., 1994. Interaction between aqueous uranium(VI) and sulfide minerals – spectroscopic evidence for sorption and reduction. Geochim. Cosmochim. Acta 58 (13), 2829–2843.
WoldeGabriel, G., Boukhalfa, H., Ware, S.D., Cheshire, M., Reimus, P., Heikoop, J., Conradson, S.D., Batuk, O., Havrilla, G., House, B., Simmons, A., Clay, J., Basu, A., Christensen, J.N., Brown, S.T., DePaolo, D.J., 2014. Characterization of cores from an in-situ recovery mined uranium deposit in Wyoming: implications for post-mining restoration. Chem. Geol. 390, 32–45.
World Nuclear Association, 2014. In Situ Leach (ISL) Mining of Uranium (London, United Kingdom). http://www.world-nuclear.org/info/Nuclear-Fuel-Cycle/Mining-of-Uranium/In-Situ-Leach-Mining-of-Uranium/ (accessed 08.09.15.).
Zielinski, R.A., Budahn, J.R., 1998. Radionuclides in fly ash and bottom ash: improved characterization based on radiography and low energy gamma-ray spectrometry. Fuel 77 (4), 259–267.